Hindawi
Journal of Chemistry
Volume 2022, Article ID 7313899, 12 pages
https://doi.org/10.1155/2022/7313899

Research Article

Waste-Tire-Derived Activated Carbon as Efficient Adsorbent of P-Nitrophenol from Wastewater

Chunhua Hu,[1] **Suliu Hu**,[1,2,3] **Ping Fang**,[2,3] **Zijun Tang**,[2,3] **Xiang Xiao**,[2,3] **and Haiwen Wu**[2,3]

[1]*Key Laboratory of Poyang Lake Environment and Resource Utilization Ministry of Education, School of Resources Environmental and Chemical Engineering, Nanchang University, Nanchang 330031, China*
[2]*South China Institute of Environmental Sciences, Ministry of Ecology and Environment, Guangzhou 510655, China*
[3]*The Key Laboratory of Water and Air Pollution Control of Guangdong Province, Guangzhou 510655, China*

Correspondence should be addressed to Ping Fang; fangping@scies.org

Received 27 October 2021; Revised 8 January 2022; Accepted 15 January 2022; Published 15 February 2022

Academic Editor: Gomaa A. M. Ali

In this work, a two-stage activation method was used to prepare adsorbents from scrap tire rubber. Firstly, KOH was mixed with rubber using different impregnation ratios (1–2) for primary activation; a second activation was performed after pyrolysis at 650°C and 750°C; and finally, the samples were acid-washed using HNO_3. The prepared materials were characterized by elemental analysis, nitrogen adsorption isotherms, SEM, FTIR, and XPS. The adsorption capacity and mechanism of these materials on p-nitrophenol in wastewater were also investigated. It was found that after two-stage activation, the specific surface area of the materials can be effectively increased, and the surface of the materials can be enriched with oxygen-containing functional groups. The maximum adsorption capacity of PNP could reach 143.9 mg g^{-1}, which is slightly higher than the literature data under the same conditions. The adsorption process is in the form of chemisorption and is dominated by hydrogen bonding and π-πEDA formation, but the adsorption tends to be monolayer, and the adsorption behavior can be described by a proposed secondary model. In addition, the adsorbent has a stronger adsorption capacity under acidic conditions.

1. Introduction

With the economic take-off and the development of the automobile industry, the number of waste tires produced every year in China has increased sharply at a rate of 8%–10% in recent years, which has become a new type of pollution [1]. The main difficulty in the disposal of waste tires is that the tires occupy a large amount of environmental space and are difficult to compress, collect, and eliminate [2]. In view of the uncertainty in the time required for the decomposition of old tires, they are not biodegradable, and their composition includes some dangerous elements, such as lead, chromium, cadmium, and other heavy metals [3]. If not handled and properly managed, they will threaten the natural environment and human health. Thus, it is urgent to control the "black pollution" caused by waste tires [4].

There are three main recycling methods for waste tire rubber treatment, the first of which is scrap tire retreading, which is considered to delay the ultimate solution [5]. However, the second method is thermal energy utilization, where scrap tires are treated as fuel alone or mixed with other combustible materials. Despite the simplicity of combustion to recover thermal energy, it can contribute to air pollution. The third one is the new thermochemical utilization such as pyrolysis technology. Pyrolysis is considered a promising method for the thermochemical treatment of waste tires [6]. Through reactions under negative or atmospheric pressure, carbon black, fuel oil, and a small amount of noncondensable gas can be obtained for resource utilization of scrap tires [7].

If waste tires can be used as raw material to produce activated carbon, it will help reduce the consumption of raw materials. This is reflected in the fact that biomass is currently the main raw material for the preparation of activated carbon, and the rapid extension of the global activated carbon market from 2016 to 2022 may be restrained by

factors such as raw material shortage [1]. As a material with high carbon content, pyrolytic carbon black has a preliminary pore structure, which can be further developed by proper activation treatment. The applications of pyrolytic carbon as a substitute for carbon black in the rubber industry [8], biochar for soil improvement [9], and activated carbon for pollution control have made the corresponding progress [10].

Also, as nitroaromatic compounds are released into the environment through the manufacture of fine chemical intermediates, these intermediates are widely used in dyes, explosives, leather preservatives, pesticides, and medical drugs [11]. P-nitrophenol (PNP) is a representative nitroaromatic compound with high chemical stability and high biological toxicity [12]. It is recognized by the US Environmental Protection Agency as one of the most persistent, bioaccumulative, and toxic chemicals [13]. It is essential to pay attention to the generation and elimination of these pollutants. Therefore, it was used as a simulated pollutant for this study. Currently, microbial treatment [14], photochemical oxidation [15], and adsorption [16, 17] are widely used to remove organic matter from wastewater. However, the adsorption method relying on activated carbon or other adsorbents has the advantages of simple operation, high treatment capacity, and no need to add other chemicals for the treatment of phenolic compounds [18, 19]. Therefore, it has a broad prospect in the treatment of organic pollutants in water.

In this paper, the methods of activating waste tires by chemical activation and pickling after reheating are presented. Waste tires were mixed with KOH in different proportions and then heated at different temperatures to increase the pores on the rubber surface of the waste tires. Then, by nitric acid pickling, tar and other substances attached to the surface of rubber-activated carbon (RAC) were removed, and oxygen-containing functional groups on the surface of RAC increased. The other four activated carbons were prepared by this method and formed a contrast. Using PNP as an adsorbent, the effects of different ratios of KOH and temperature on adsorption were investigated. The equilibrium and kinetics of RAC adsorption were studied. The adsorption properties of RAC on PNP were compared with those in the literature, and the differences in pore structure and surface chemistry were explained by infrared spectroscopy, BET, BJH, and other methods. This paper provides a new idea for the treatment of waste tire resources, which is helpful to solve the problem of PNP simultaneous pollution of solid waste and wastewater.

2. Materials and Methods

2.1. Preparation and Modification/Activation of Rubber Activated Carbon. The tire rubber was crushed in a waste tire treatment plant in Guangxi Province, China, and used as raw material. After screening, particles with a particle size of 0.15–0.45 mm were selected as experimental samples. Analytical pure KOH (Guangzhou Chemical Reagent Factory), analytical pure p-nitrophenol (Xiya Reagent), and treated tire rubber were used as reference materials for adsorption experiments.

The preparation methods of five kinds of RAC and their numbers are shown in Table 1.

The preparation of 650-2 is mainly by premixing waste tire rubber powder with KOH at a dipping ratio of 1:2, soaking for 12 h, using a vacuum pump to remove the water, and then drying at 80°C in a blast drying oven for 6 h until the activation of KOH is completed. Then the horizontal tubular furnace was preheated to 650°C with a nitrogen flow rate of 1.5 L h^{-1}, and the samples were placed in the tubular furnace for 1 h before being taken. Finally, the samples were soaked in 20% HNO_3 for 12 h, dried, and sealed for preservation.

2.2. Materials Characteristics. The elements (carbon (C), hydrogen (H), nitrogen (N), and sulfur (S)) and components of the prepared activated carbon were measured and analyzed by an element analyzer (EA3000, Euro Vector, Italy). Dried samples of about 1–2 mg were taken to analyze the total of C, H, N, and S. The total oxygen (O) is determined by the following formula [20, 21]:

$$O(\%) = 100 - ash(\%) - C(\%) - N(\%) - H(\%). \quad (1)$$

Activated carbon pore structure was determined by the American company Michael ASAP-2020 instrument automatically physisorption. The adsorption isotherm of activated carbon for nitrogen was measured at 77 K with nitrogen as the adsorbent, which was used to calculate the specific surface area and pore structure size of the carbon. The sample was degassed at 120°C for 6 h before testing. The specific surface area of activated carbon by BET (Brunauer–Emmett–Teller) method of calculation adopting BJH (Barrett–Joyner–Halenda) pore size distribution was measured on a model of the desorption branch.

Activated carbon surface morphology was observed by Japan's JSM-5600 scanning electron microscope (SEM).

The Fourier transform infrared spectrometer (Nicolet IS10) was used to determine the spectral characteristics of activated carbon and the composition of functional groups on the surface of activated carbon samples.

Each experiment was performed three times repeatedly; all results are the average of three replicate experiments; and the relative error is guaranteed to be less than 5%. The agents and instruments used in the experiments are shown in Tables S1 and S2.

2.3. Adsorption Experiments

2.3.1. Adsorption Kinetics Experiment. The adsorption kinetics experiment was carried out in a 150 ml conical flask at 25°C, adding 20 mg sample and 50 ml PNP solution. Unless otherwise stated, the solution was shaken in a reciprocating + gyroscopic constant temperature shaker (YAWL-280BCF) at 120 RPM for 36 h to ensure adsorption equilibrium. After the adsorption equilibrium, it was filtered through a 0.45 μm membrane filter. A 317 nm UV-vis spectrophotometer (UV-5100, Shanghai) was used to determine the concentration of PNP in the aqueous solution. The adsorption capacity and adsorption efficiency of

Table 1: Simplified version of five RAC preparation methods.

Activated carbon number	Preparation
650-0	Pyrolyzed at 650°C, sieved, washed with water, and dried at 80°C
650-1	KOH impregnation ratio 1:1, dried at 80°C. Pyrolyzed at 650°C for 1 h, sieved, washed with water to neutrality, and dried at 80°C
650-2	KOH impregnation ratio 1:2, dried at 80°C. Pyrolyzed at 650°C for 1h, sieved, pickled for 12 h, washed with water to neutrality, and dried at 80°C
750-1	KOH impregnation ratio 1:1, dried at 80°C. Pyrolyzed at 750 °C for 1 h, sieved, washed with water to neutrality, and dried at 80°C.
750-2	KOH impregnation ratio 1:2, dried at 80°C. Pyrolyzed at 750°C for 1 h, sieved, pickled for 12 h, washed with water to neutrality, and dried at 80°C.

activated carbon for PNP were calculated by the following equations [20]:

$$q_e = \frac{(C_e - C_0)}{M} * V, \tag{2}$$

$$R = \frac{(C_e - C_0)}{C_0}, \tag{3}$$

where C_e is the concentration of adsorbate at adsorption equilibrium (mg L^{-1}), C_0 is the initial concentration of adsorbate (mg L^{-1}), M is the mass of adsorbent (g), and V is the volume of solution (mL).

2.3.2. Isothermal Adsorption Experiment. The isothermal adsorption experiment was conducted by adding 0.2 g 650-2 to 50 mL PNP solution with different concentrations (10–500 mg L^{-1}) at a constant speed of 120 RPM at 25°C for 12 h.

The kinetic and isothermal adsorption data were fitted with related models. $\chi 2$ and correlation degree R^2 are commonly used to evaluate the goodness of fit of the equation and experimental data as follows [20]:

$$\chi^2 = \sum \left(\frac{\left(q_{exp} - q_{mo\,d}\right)^2}{q_{mo\,d}} \right), \tag{4}$$

where q_{exp} is the adsorption capacity calculated from the experimental data and q_{mod} is the adsorption capacity calculated from the model.

2.3.3. Effect of pH on Adsorption. To study the effect of pH on the adsorption of 650-2 PNP, the experiment was carried out under the condition of pH 2–12.0.2 g 650-2 was added to 50 mL PNP (100 mg L^{-1}) solution, and the pH of the solution was adjusted with NaOH and HCl. Finally, the glass bottle was shaken in a 25°C constant temperature water bath shaker at 120 RPM for 12 h.

3. Results and Discussion

3.1. Characterization of Rubber Activated Carbon. The yield equation is as follows [22]:

$$Y = \frac{m}{M}, \tag{5}$$

where Y is the yield, M is the final mass of the sample, and m is the initial mass of the sample.

C, H, O, and N elements are the main elements of the carbon skeleton and surface functional groups. H/C, O/C, and (N + O)/C are aromatic, hydrophilic, and polar indexes, respectively [23]. At the same pyrolysis temperature, the yield of activated carbon KOH decreased significantly. It is because KOH is reduced to potassium at high temperatures, and K can promote the oxidation of tire rubber to CO and CO_2 [24]. Simultaneously, the formation of pores is accelerated, resulting in the loss of activated carbon [20]. Table 2 also shows that the three carbons produced at 650°C are solids rich in carbon, and the carbon content at 750°C is less, which may be due to the high temperature in the pyrolysis process, leading to a large amount of carbon loss. From Table 2, 650-2 has the best aromatization, certain hydrophilicity, and good polarity. Compared with 650-1, after pickling, 650-2 (H/C: 0.02, O/C: 0.22, and (N + O)/C: 0.12) has enhanced aromatization and weakened hydrophilicity and polarity [25].

3.2. Specific Surface Area and Pore Size Distribution. Figure 1 shows the 650-2 adsorption of N_2, desorption curve, and found that 650-2 adsorption isotherms were "IV" type [26], having a concave isotherm without inflection. The amount of adsorbed gas increased as the component partial pressure increased. Based on the pore size distribution in the figure, the pore size of the 650-2 is mainly concentrated on the outer surface. The characteristics of 650-2 shown here can be mutually supported by the single-layer adsorption of p-nitrophenol in isothermal adsorption experiments. The nitrogen adsorption/desorption curves and pore size distributions of the remaining four activated carbons are shown in Figures S1, S2, S3, and S4. Their nitrogen adsorption/desorption curves and pore size distributions were similar to that of 650-2.

Based on Table 3, the change of specific surface area between 650-0 and 650-1 shows that the increase of KOH proportion can indeed increase and promote the growth of the specific surface area. According to the changes of specific surface area, pore volume, and average pore size of activated carbon at 650°C and 750°C, the pore size can be increased with the increase of temperature, but the surface structure will be affected. From the results of comprehensive pore size and specific surface area, 650-2 provides a sufficient adhesion surface for PNP.

Table 2: The elements C, N, H, and O are present in five kinds of RAC.

Sample	Impregnation ratio	Y_a (%)	Elemental analysis (wt.%)					Atomic ratio		
			N	C	H	O	Ash	H/C	O/C	(N + O)/C
650-0	—	78	0.420	74.72	1.177	5	16.454	0.02	0.07	0.07
650-1	1:1	63	0.380	81.03	4.286	5.41	7.38	0.03	0.13	0.14
650-2	1:2	54	0.640	79.01	1.587	8.49	7.878	0.02	0.11	0.12
750-1	1:1	61	0.460	40.26	2.275	23.55	31.492	0.06	0.58	0.60
750-2	1:2	52	0.800	42.47	1.28	23	30.179	0.05	0.28	0.29

The yield equation is shown below [22].

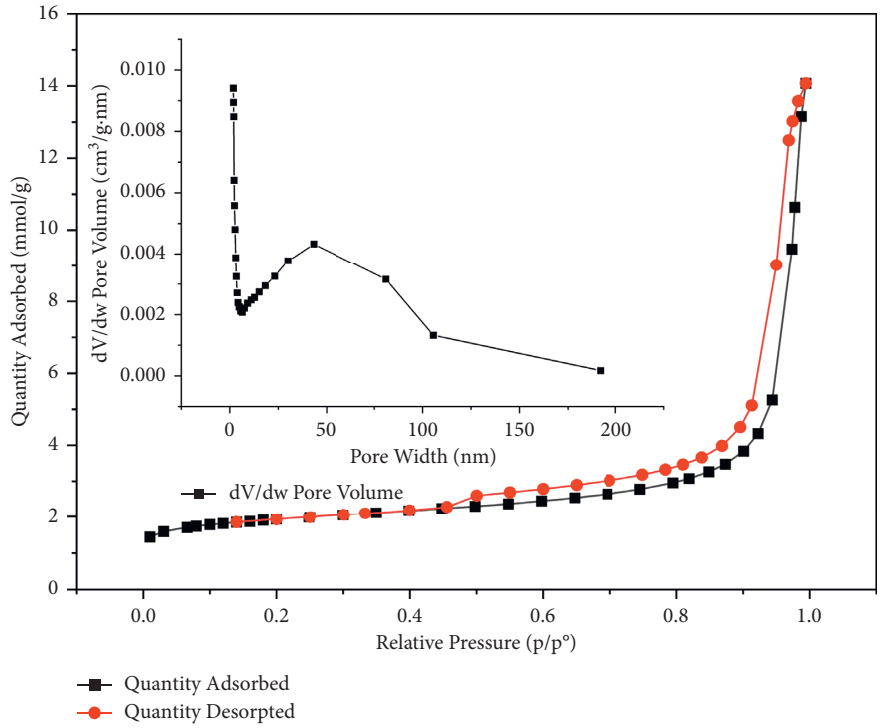

Figure 1: N_2 adsorption/desorption isotherms and pore size distributions of 650-2.

Table 3: Physical adsorption characterization results of five types of carbon.

Sample	S_{BET}[a] ($m^2\ g^{-1}$)	V_{MIC}[b] ($cm^3\ g^{-1}$)	APD[c] (nm)
650-0	19.77	0.0016	20.8404
650-1	76.96	0.0035	17.5035
650-2	150.49	0.034	8.7976
750-1	13.11	0.0017	31.36028
750-2	11.79	0.0016	34.10843

[a]BET surface area, [b]t-plot micropore volume, and [c]adsorption average pore diameter (4 V/A by BET).

3.3. Surface Morphological Structure. Figure 2 shows the difference in surface morphology of the five activated carbons. According to Figure 2, the sample size is basically between 0.4 and 0.8 μm. The surfaces of the washed activated carbon 650-0 and 650-1 were a blocky structure, with thick pore walls, few pores, and a mass of fragments dispersed in them. However, the particle structure of 750-1 was relatively complete; the biomass left in the pore has been greatly reduced; and a large number of irregular voids have been formed. Although an increase in temperature was effective in removing debris from the pores, tar in the pores still caused the internal voids to fail to fully open, limiting porosity [27]. 650-2 had a relatively complete block structure. A great number of connected large holes were formed on the surface, and some substances around the holes were separated with a clear structure. After activation, heating and then pickling could help remove tar from the carbon surface [28]. Compared with the pore state, the specific surface area of 650-2 activated carbon was significantly higher than that of the other four, and BET analysis confirmed this phenomenon.

3.4. FTIR Analysis. To further study the properties of the adsorbent, five types of carbon were analyzed by FTIR. The transmission spectrum between 500 and 4,000 cm^{-1} was recorded (Figure 3). The peak around 1,400 cm^{-1} is the characteristic peak of –C–O [29], and the peak around 1,230 cm^{-1} is generally considered to be caused by C–O

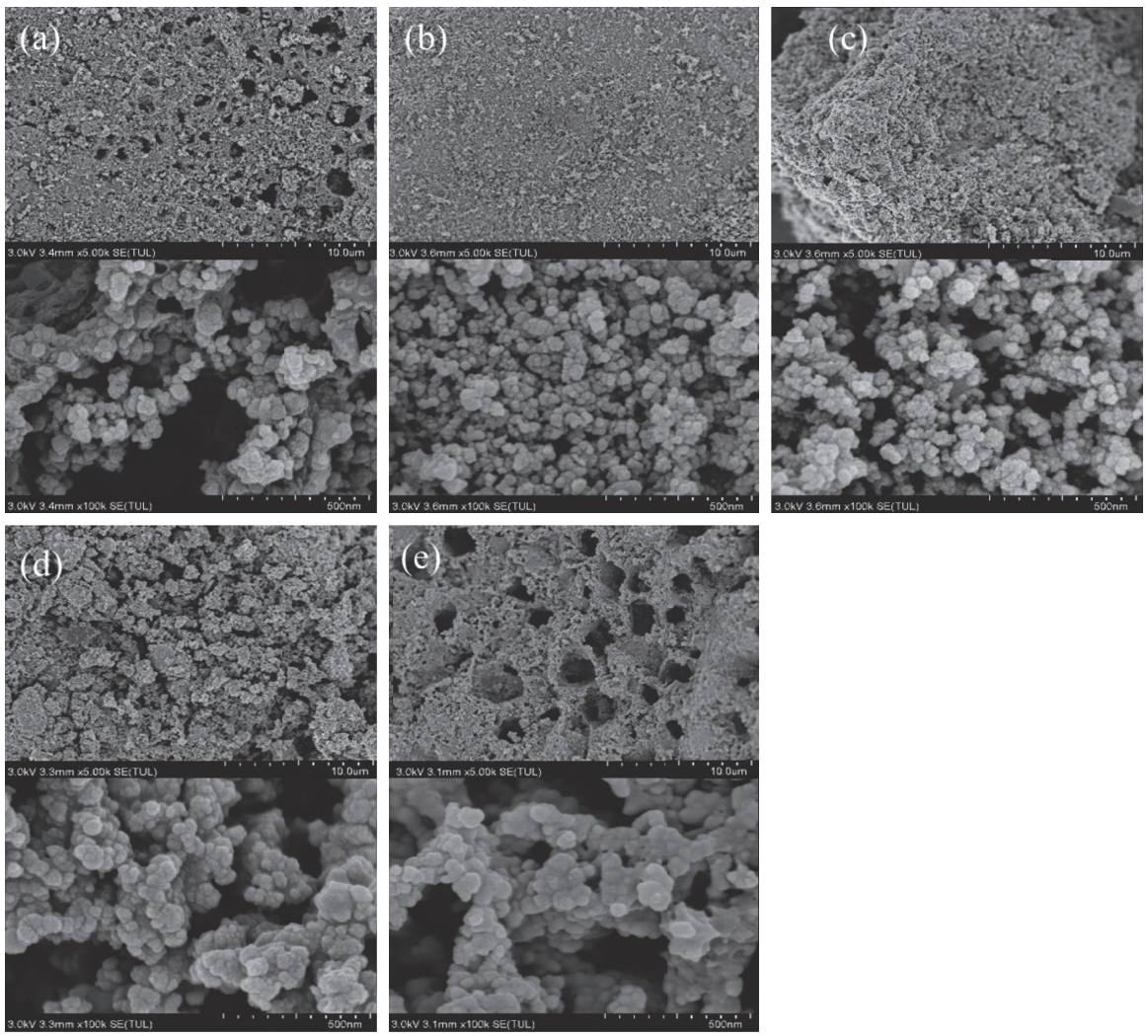

Figure 2: SEM spectrum of five activated carbon samples: (a) 650-2, (b) 650-0, (c) 650-1, (d) 750-1, and (e) 750-2.

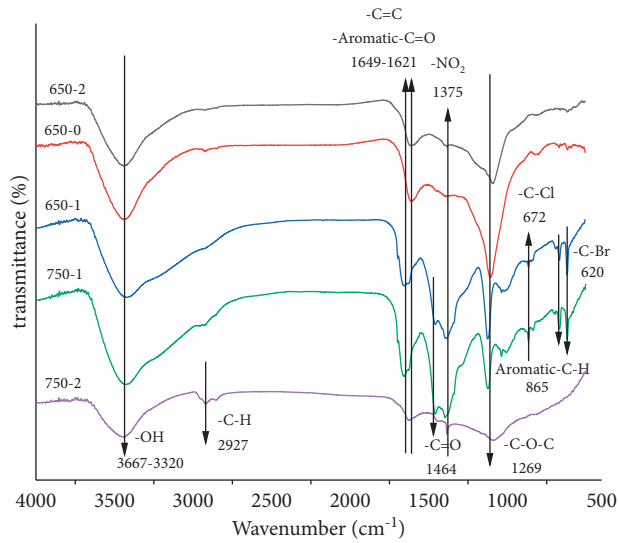

Figure 3: Fourier infrared spectra of activated carbon samples.

vibration [30]. The other peaks in the range of 951, 1,000–1,300 cm^{-1} correspond to C–C in esters, ethers, or phenols, and many characteristic peaks between 700 and 900 cm^{-1} are considered to be related to the aromatic structure [31]. Therefore, it is demonstrated that the RAC is rich in oxygen-containing functional groups, and the activated carbon after two-stage activation has more oxygen-containing functional groups (C–O–C, C=O) than the one-stage activated carbon. Besides, after the first stage of activation, the nitro group peak of rubber is obvious, and the surface activity of carbon increases. Moreover, with the decrease in the strength of the C=O or C–O–C group, the rubber and water were further separated after activation of the two stages; the hydrogen bond was broken; and the hydrophilicity of carbon was reduced. The hydroxyl and nitro groups in the carbon were gradually reduced by two stages of activation. Thus, the polarity weakened, increasing the degree of aromatization [32]. However, in comparison, as shown in the figure, the peak intensity of –OH and C–O–C of 650-2 is higher. Therefore, the polarity and hydrophilicity of 650-2 are better than those of the other four activated carbons, which correspond to the results of the elemental analysis.

3.5. XPS Analysis. In order to explore the changes of oxygen-containing functional groups in 650-2 before and after adsorption, XPS analysis was performed on carbon and oxygen elements, and the high-resolution C1s peaks were decomposed into the following three separate peaks: graphitized carbon at 284.2–284.9 eV, C–O– at 285.9 eV, and π-Nπ^* transition at 290.1 eV [33, 34]. High-resolution O1 s peaks are decomposed into the following three separate peaks: 531.4–530.9 eV OH–, 531.9–532.6 eV C=O–, and 533.1–533.5 eV C–O–[35].

According to Figure 4, the π-Nπ^* transition peaks disappear after adsorption, while the binding energies of C–O– and C=O– move significantly to higher regions. This is due to the interaction of the benzene ring of PNP with 650-2 viaπ-πEDA [36]. In addition, from Table 4, –OH, –COOH, and other functional groups on the 650-2 surface can form hydrogen bonds with several H-containing groups of PNP molecules, and the participation of the bonds in the adsorption process of PNP is confirmed [37]. The results of XPS analysis showed the presence of chemisorption of 650-2 on PNP, but the adsorption process was not necessarily controlled mainly by chemical interactions.

3.6. Kinetics of p-Nitrophenol Adsorption. The influence of adsorption contact time between RAC and PNP is shown in Figure 5. Only 650-2 could reach 85% of the maximum adsorption capacity of PNP within 1 h and then tend to slow down after 5 h and reach equilibrium within 24 h. Except for 650-0, the adsorption equilibrium time was almost the same. From Figure 5, the equilibrium adsorption capacities of PNP on 650-2, 650-0, 650-1, 750-1, and 750-1 with pseudo-first-order kinetic results were 64.7 mg g^{-1}, 38.67 mg g^{-1}, 24.78 mg g^{-1}, 31.61 mg g^{-1}, and 42.66 mg g^{-1}, respectively. The results show that the adsorption capacity of the RAC prepared by the two-stage activation method is higher than that of the activated carbon prepared by other methods at 650°C for PNP [16]. Therefore, the RAC prepared by a two-stage activation method at 650°C can be used as a promising PNP adsorbent.

Figure 6 shows the adsorption capacity and removal efficiency of 650-2 for PNP under different initial concentrations (10–500 mg L^{-1}) at 25°C. The adsorption capacity of 650-2 increased with the increase of the initial concentration of PNP until it reached adsorption saturation. As the amount of activated carbon used was constant, with the concentration of PNP in the solution increased, the removal rate of PNP decreased, but the absolute adsorption capacity and the saturated adsorption capacity of the carbon for PNP increased.

In order to study the adsorption efficiencies of five kinds of carbon, three different kinetic methods were used, namely, pseudo-first-order kinetic equation, pseudo-second-order kinetic equation, and intraparticle diffusion kinetic model. The specific citation features and performance are as follows:

Pseudo-first-order kinetic equation is as follows [38]:

$$\ln\left(q_e - q_t\right) = \ln\, q_e - K_1 t. \tag{6}$$

Pseudo-second-order kinetics can be expressed by the following formula [39]:

$$\frac{dq_t}{dt} = K_2\left(q_e - q_t\right)^2. \tag{7}$$

The intraparticle diffusion-reaction is as follows [40]:

$$q_t = k_{di} \cdot t^{(1/2)} + C, \tag{8}$$

where q_e is the adsorption amount at equilibrium (mg g^{-1}), K_1 (h^{-1}) is the pseudo-first-order kinetic rate constant, K_2 is the pseudo-second-order kinetic rate constants, k_{di} is a diffusion rate constant (mg (g $h^{1/2})^{-1}$), and C is a constant (mg g^{-1}).

In Tables 5 and 6, the pseudo-second-order kinetic model is in good agreement with the experimental data, and R_2 is high ($R_2 = 0.97$). Therefore, the adsorption of PNP on (650-2) carbon conforms to the quasi-second-order kinetic model, and the main control mechanism is chemisorption.

However, the purpose of further exploring the mechanism of diffusion and the control process using kinetic data fits the particle diffusion model. As shown in Figure 7(b) and Table 6, the surface diffusion constant K_{d1} is greater than the intraparticle diffusion constant K_{d2}, and the boundary layer C_2 (intraparticle diffusion) is greater than C_1 (surface diffusion). This shows that the inner surface effect of activated carbon is greater than the diffusion effect. Mainly because the activated carbon in the initial adsorption has a large number of surface adsorption sites, pollutants may temporarily use the adsorbent surface of the most easily obtained adsorption sites, to have a fast adsorption rate. The results can be supported by pore size analysis.

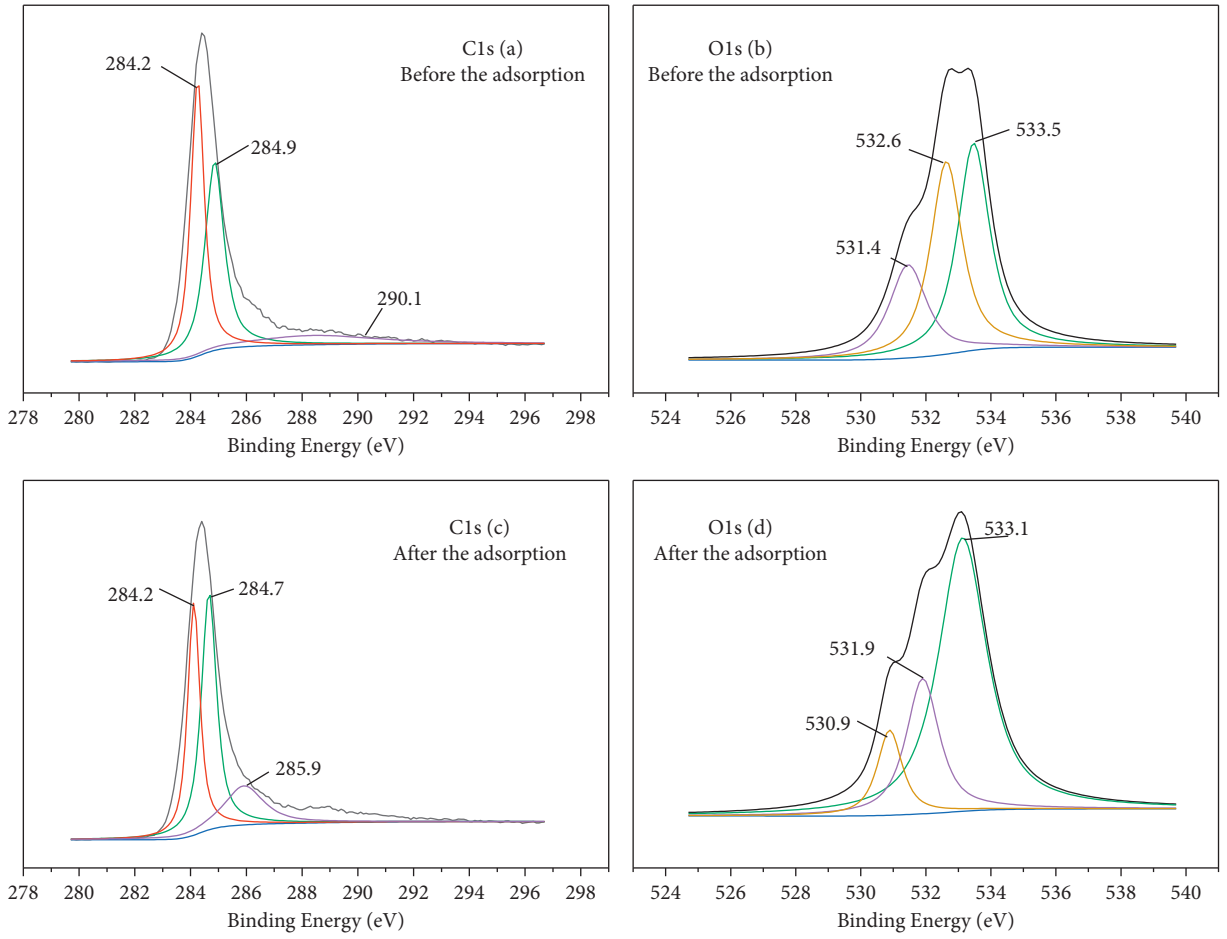

Figure 4: XPS spectra of 650-2 before and after PNP adsorption: C 1 s (a) and (c); O 1 s (b) and (d).

Table 4: Quantification of oxygen groups on 650-2 surface.

Boehm's titration	650-2
Carboxyl group (mmol g^{-1})	0.023
Lactone group (mmol g^{-1})	1.253
Phenolic group (mmol g^{-1})	0.793
Total basic groups (mmol g^{-1})	1.376

3.7. Adsorption Isotherm Analysis. This section was fitted and analyzed using the Langmuir model, Freundlich model, and Sips isothermal model for the data of [41] to investigate the relationship between activated carbon and PNP.

Langmuir isotherm model is expressed as follows:

$$q_e = \frac{K_l q_m C_e}{1 + K_L C_e}. \quad (9)$$

Freundlich adsorption isotherm is as follows:

$$q_e = K_F C_e^{(1/n)}. \quad (10)$$

Sips adsorption isotherm is as follows (11):

$$q_e = \frac{K_s q_m C_e^{(1/n)}}{1 + K_s C_e^{(1/n)}}, \quad (11)$$

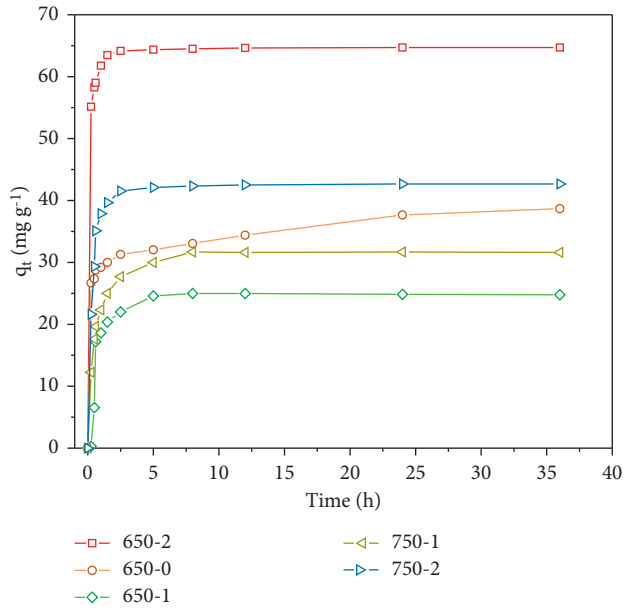

Figure 5: Comparison of the adsorption performance of five types of carbon on PNP. The initial concentration of PNP is 100 mg L^{-1} (25°C, pH = 5, C_0 = 100 mg L^{-1}, and adsorption time of 36 h).

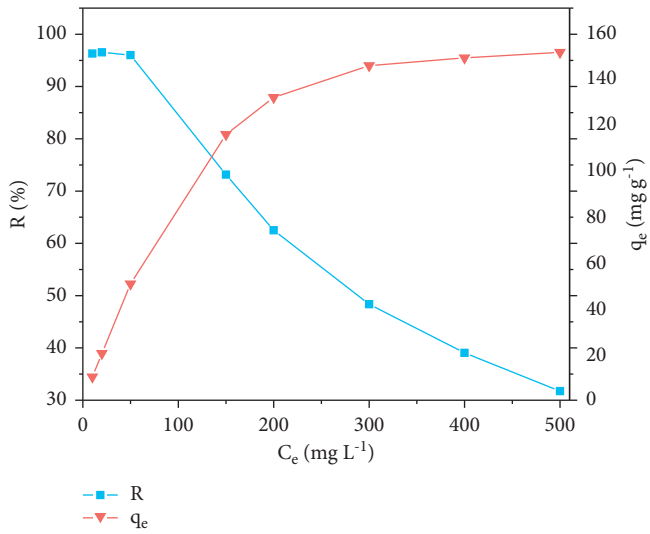

Figure 6: The adsorption capacity and removal rate of 650-2 for PNP under different initial concentrations; the initial concentration of PNP is 10–500 mg L^{-1} (25°C, pH = 5, C_0 at 10–500 mg L^{-1}, and adsorption time of 24 h).

Table 5: The analysis of pseudo-first-order and pseudo-second-order dynamics of RAC.

Absorbent	Pseudo-first-order				Pseudo-second-order			
	q_m (mg g^{-1})	K_1 (h^{-1})	R^2	χ^2	q_m (mg g^{-1})	K_2 (h^{-1})	R^2	χ^2
650-2	64.7	7.38	0.98	0.11	76.491	3.21	0.97	0.39
650-0	38.67	5.03	0.90	2.69	33.609	6.14	0.85	4.43
650-1	24.78	1.09	0.92	0.00	10.785	−2.30	0.32	7.15
750-1	31.61	1.57	0.97	0.15	26.316	−1.08	0.56	4.89
750-2	42.66	2.67	0.99	0.04	40.491	−4.36	0.74	1.96

Table 6: The analysis of five kinds of activated carbon diffusion models.

Adsorbent	Intraparticle diffusion							
	k_{d1} (mg(g^{-1} h$^{-1/2}$))	C_1 (mg g^{-1})	R^2	χ^2	k_{d2} (mg(g^{-1} h$^{-1/2}$))	C_2 (mg g^{-1})	R^2	χ^2
650-2	49.8725	199.49	0.96	17.65	0.79	63.7425	0.62	0.06
650-0	24.505	98.02	0.904	28.24	7.39	28.0075	0.99	13.30
650-1	10.745	42.98	0.79	74.03	2.9	21.4875	0.47	2.10
750-1	4.2375	16.95	0.95	463.89	3.76	21.93	0.57	3.65
750-2	10.205	40.82	0.92	251.93	1.5	33.7425	0.53	0.39

where C_e is the equilibrium adsorption concentration (mg L^{-1}), q_e is the equilibrium adsorption capacity (mg g^{-1}), K_F is the Freundlich constant ((mg g^{-1}) (mg^{-1})$^{1/n}$), K_S is the Sips model isotherm constant (L g^{-1}), and n is the exponent of this model.

As can be seen from Figure 8 and Table 7, with the increase of the initial concentration of pollutants, the adsorption capacity increases and finally tends to balance and reaches the maximum adsorption capacity. The maximum adsorption capacity of 650-2 is 143.9 mg g^{-1}. In addition, among the nonlinear fitting of the three models, the correlation coefficient (R_2) of the Sips model, the Langmuir adsorption model, and the Freundlich model were 0.997, 0.995, and 0.994, respectively. In conclusion, the adsorption of PNP at 650-2 was more consistent with Sips and Langmuir adsorption models. The results showed PNP was adsorbed on the surface of the monolayer of the adsorbent, while there was a small amount of chemisorption [42].

3.8. Effect of pH on Adsorption. The pH affects the molecular state of the pollutant and the surface chemical properties of the adsorbent. The adsorption of PNP on 650-2 was carried out in the pH range of 2–12 (Figure 9). The results showed that the adsorption capacity of 650-2 on PNP was better under acidic conditions than that under alkaline conditions. It may be that under acidic conditions, the surface of 650-2 is positively charged, and there is an electrostatic attraction between it and PNP in dissociation, which leads to an increase in adsorption efficiency. The decrease of adsorption

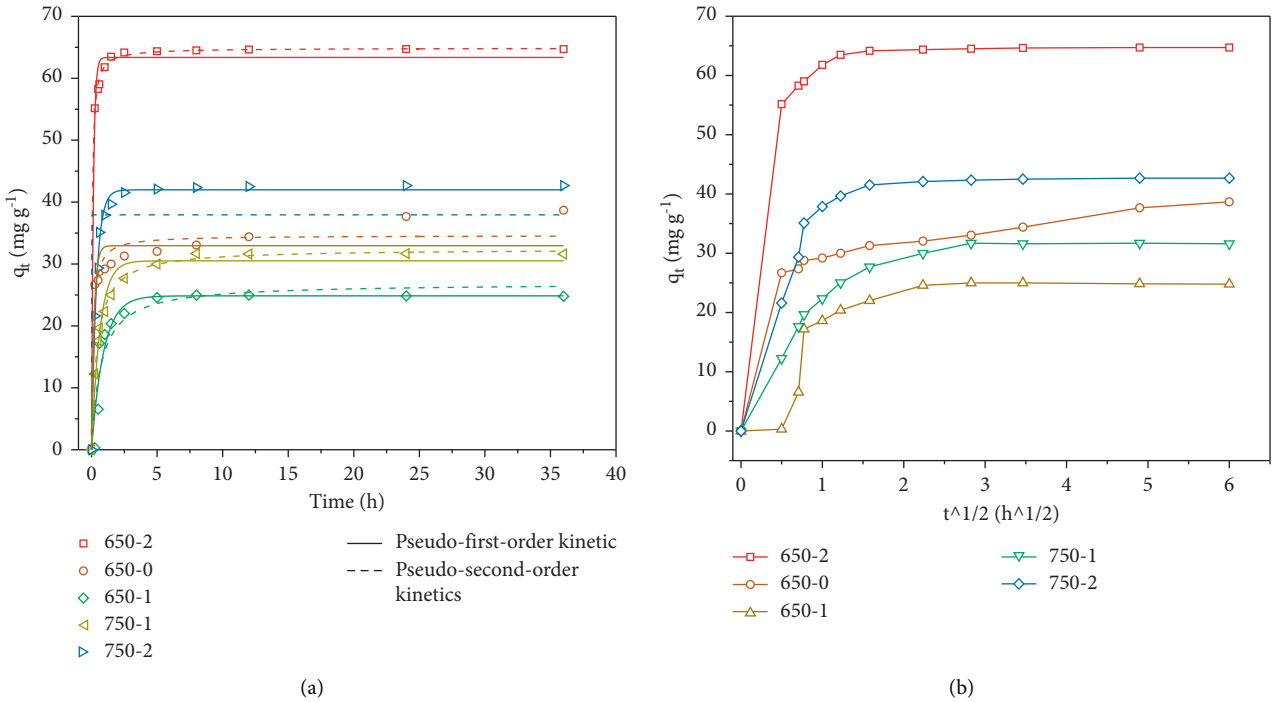

Figure 7: Fitting the adsorption kinetics of five kinds of carbon: (a) pseudo-first-order kinetic equation and pseudo-second-order kinetic equation and (b) internal diffusion model (25°C, pH = 5, C_0 at 10–500 mg L^{-1}, and adsorption time of 24 h).

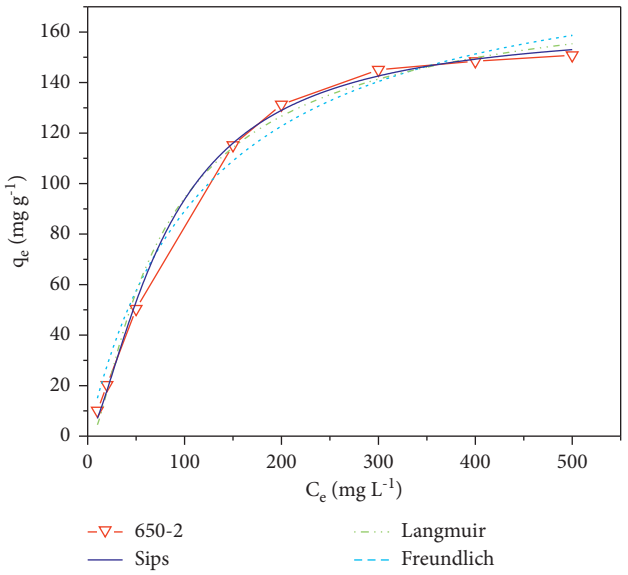

Figure 8: Representation of the linear form of the Langmuir, Freundlich, and Sips model isotherm adsorption model.

Table 7: The parameter of the Langmuir, Freundlich, and Sips model isotherm for PNP adsorption on 650-2.

Langmuir Parameters		Freundlich Parameters		Sips Parameters	
q_m (mg g^{-1})	197.18	K_F (mg g^{-1})	172.2	q_m (mg g^{-1})	163.9
K_L (L mg^{-1})	0.008	n	0.96	K_s (L g^{-1})	0.003
R^2	0.995	R^2	0.994	n	2.12
χ^2	0.008	χ^2	0.009	R^2	0.997
				χ^2	0.0001

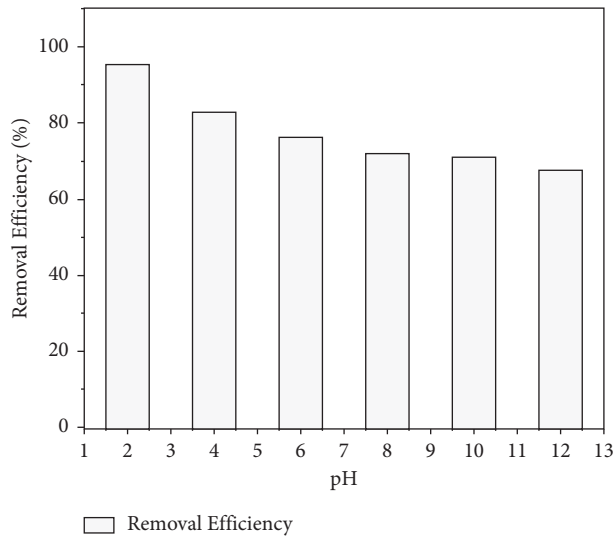

Figure 9: Effect of pH on the adsorption of PNP on 650-2 (25°C, pH at 2–12, C_0 at 10–500 mg L^{-1}, and adsorption time of 24 h).

Table 8: The properties of some adsorbents and their adsorption performance for PNP.

Adsorbing agent	q_e (mg g^{-1})	Adsorption saturation time (h)	Temperature (°C)	Source
650-2	64.7	6	25	This paper
650-1	38.67	6	25	This paper
650-0	24.78	6	25	This paper
750-1	31.61	6	25	This paper
750-2	42.66	6	25	This paper
AB	49.25	12	25	[39]
Mansonia wood sawdust	18	2	24	[40]
Amides	65.78	2	25	[44]
Activated carbon from carrot dross	24.37	2	25	[37]
PAN–ACF/ZnO	23.8039	48	25	[45]

efficiency under alkaline conditions may be caused by the competitive adsorption between PNP and H_3O^+ ions [43].

3.9. Comparative Study of 650-2 with Other Adsorbents. Other scholars have also carried out studies on the adsorption performance of activated carbon on phenol, p-nitrophenol, and o-nitrophenol. Table 8 shows the research results of this article and related scholars. According to the comparison of the experimental results, it is found that 650-2 as an adsorbent has higher efficiency on PNP. In this experiment, the activated carbon with rubber as the precursor has a high adsorption capacity for PNP, and 650-2 ranks first among them. And the adsorption capacity of RAC for PNP also reached a strong level. Therefore, RAC has good prospects for application in the field of adsorption.

4. Conclusion

In this proposed method, after two stages of activation with waste tire rubber, it was determined that for waste tire rubber, the temperature did not seem to be positively correlated with the results of normal material preparation similarly. However, the increase of impregnation ratio does effectively improve the specific surface area and pore size of the material. If a higher specific surface area is needed guess that it can be achieved by increasing the impregnation ratio. The material has a complete bulk structure, well-defined pore size, specific surface area at 150.49 $m^2 g^{-1}$, and abundant oxygen-containing functional groups on the surface.

In the application of p-nitrophenol wastewater adsorption, the adsorption of PNP was good and greater under acidic conditions, probably due to the positively charged surface due to hydrogen bonding under acidic conditions, and the adsorption kinetics can be described by a secondary model, where the adsorption mechanism is monolayer adsorption and chemisorption, mainly due to the combined effect of hydrogen bonding and π-πEDA.

Data Availability

The authors acknowledge that data supporting the results of this study can be found in the article. Data related to the study are available from the authors upon request.

Conflicts of Interest

The authors declare that they have no conflicts of interest.

Supplementary Materials

Table S SEQ Table \∗ ARABIC 1: The name of the drug required for the experiment, its specification and purity, and the manufacturer; Table S SEQ Table \∗ ARABIC 2: Main

experimental equipment and analytical testing instruments; Figure S SEQ Figure \∗ ARABIC 1: N_2 adsorption/desorption isotherms and pore size distributions of 650-0; Figure S SEQ Figure \∗ ARABIC 2: N_2 adsorption/desorption isotherms and pore size distributions of 650-1; Figure S SEQ Figure \∗ ARABIC 3: N_2 adsorption/desorption isotherms and pore size distributions of 750-1; and Figure S SEQ Figure \∗ ARABIC 4: N_2 adsorption/desorption isotherms and pore size distributions of 750-2. (*Supplementary Materials*)

References

[1] J. Xu, J. Yu, J. Xu et al., "High-value utilization of waste tires: a review with focus on modified carbon black from pyrolysis," *The Science of the Total Environment*, vol. 742, Article ID 140235, 2020.

[2] S. H. Brandsma, M. Brits, Q. R. Groenewoud, M. J. M. van Velzen, P. E. G. Leonards, and J. de Boer, "Chlorinated paraffins in car tires recycled to rubber granulates and playground tiles," *Environmental Science and Technology*, vol. 53, no. 13, pp. 7595–7603, 2019.

[3] A. N. Perkins, S. H. Inayat-Hussain, N. C. Deziel et al., "Evaluation of potential carcinogenicity of organic chemicals in synthetic turf crumb rubber," *Environmental Research*, vol. 169, pp. 163–172, 2019.

[4] B. S. Thomas, R. C. Gupta, and V. J. Panicker, "Recycling of waste tire rubber as aggregate in concrete: durability-related performance," *Journal of Cleaner Production*, vol. 112, pp. 504–513, 2016.

[5] A. A. Hassan, K. Formela, and S. Wang, "Reclaimed rubber in situ grafted with soybean oil as a novel green reactive plasticizer in SBR/silica compounds," *ACS Sustainable Chemistry & Engineering*, vol. 7, no. 17, pp. 14991–15001, 2019.

[6] M. Benedetti, L. Cafiero, D. D. Angelis et al., "Pyrolysis of WEEE plastics using catalysts produced from fly ash of coal gasification," *Frontiers of Environmental Science & Engineering*, vol. 11, pp. 110–120, 2017.

[7] R. Kommineni, H. Boddapu, and S. Thomas, *Scope of Pyrolysis Process as a Sustainable Method to Dispose Waste Tires: A Review*, Springer, Singapore, 2018.

[8] X. Zhang, H. Li, Q. Cao, L. Jin, and F. Wang, "Upgrading pyrolytic residue from waste tires to commercial carbon black," *Waste Management & Research*, vol. 17, 2018.

[9] K. F. Mendes, G. P. Olivatto, R. N. de Sousa, L. V. Junqueira, and V. L. Tornisielo, "Natural biochar effect on sorption-desorption and mobility of diclosulam and pendimethalin in soil," *Geoderma*, vol. 347, pp. 118–125, 2019.

[10] A. Trubetskaya, J. Kling, O. Ershag, T. M. Attard, and E. Schröder, "Removal of phenol and chlorine from wastewater using steam activated biomass soot and tire carbon black," *Journal of Hazardous Materials*, vol. 365, pp. 846–856, 2019.

[11] H. Zhu, X. Ke, X. Yang, S. Sarina, and H. Liu, "Reduction of nitroaromatic compounds on supported gold nanoparticles by visible and ultraviolet light," *Angewandte Chemie International Edition*, vol. 49, no. 50, pp. 9657–9661, 2010.

[12] Rickert. Toxicity of Nitroaromatic Compounds. 1985.

[13] J. Liu, "Toxicities of nitroaromatic compounds to scenedesmus obliquus and toxic symptoms," *Huanjing Kexue*, vol. 16, pp. 7–10, 1995.

[14] M. Li, D. Wei, L. Yan et al., "Aerobic biodegradation of p-nitrophenol in a nitrifying sludge bioreactor: system performance, sludge property and microbial community shift," *Journal of Environmental Management*, vol. 265, Article ID 110542, 2020.

[15] K. Roy and V. S. Moholkar, "p-nitrophenol degradation by hybrid advanced oxidation process of heterogeneous Fenton assisted hydrodynamic cavitation: discernment of synergistic interactions and chemical mechanism," *Chemosphere*, vol. 283, Article ID 131114, 2021.

[16] V. K. Gupta, A. Nayak, S. Agarwal, and I. Tyagi, "Potential of activated carbon from waste rubber tire for the adsorption of phenolics: effect of pre-treatment conditions," *Journal of Colloid and Interface Science*, vol. 417, pp. 420–430, 2014.

[17] Y. Rong and R. Han, "Adsorption of p-chlorophenol and p-nitrophenol in single and binary systems from solution using magnetic activated carbon," *Korean Journal of Chemical Engineering*, vol. 36, no. 6, pp. 942–953, 2019.

[18] K. Li, M. Zhou, L. Liang, L. Jiang, and W. Wang, "Ultrahigh-surface-area activated carbon aerogels derived from glucose for high-performance organic pollutants adsorption," *Journal of Colloid and Interface Science*, vol. 546, pp. 333–343, 2019.

[19] S. Liu, C. Lai, B. Li et al., "Role of radical and non-radical pathway in activating persulfate for degradation of p-nitrophenol by sulfur-doped ordered mesoporous carbon," *Chemical Engineering Journal*, vol. 384, Article ID 123304, 2020.

[20] R. Acosta, V. Fierro, A. Martinez de Yuso, D. Nabarlatz, and A. Celzard, "Tetracycline adsorption onto activated carbons produced by KOH activation of tyre pyrolysis char," *Chemosphere*, vol. 149, pp. 168–176, 2016.

[21] J. He, R. Lin, H. Long, Y. Liang, and Y. Chen, "Adsorption characteristics of amino acids on to calcium oxalate," *Journal of Colloid and Interface Science*, vol. 454, pp. 144–151, 2015.

[22] R. Acosta, V. Fierro, A. Martinez de Yuso, A. Celzard, and A. Celzard, "Tetracycline adsorption onto activated carbons produced by KOH activation of tyre pyrolysis char," *Chemosphere*, vol. 149, pp. 168–176, 2016.

[23] B. Chen and Z. Chen, "Sorption of naphthalene and 1-naphthol by biochars of orange peels with different pyrolytic temperatures," *Chemosphere*, vol. 76, no. 1, pp. 127–133, 2009.

[24] L. Fei, Z. Song, Z. Liu, L. Zhu, and B. Xing, "Mechanistic understanding of tetracycline sorption on waste tire powder and its chars as affected by Cu2+ and pH," *Environmental Pollution*, vol. 178C, pp. 264–270, 2013.

[25] D. Tang, Z. Zheng, K. Lin, J. Luan, and J. Zhang, "Adsorption of p-nitrophenol from aqueous solutions onto activated carbon fiber," *Journal of Hazardous Materials*, vol. 143, no. 1-2, pp. 49–56, 2007.

[26] Sing and K. Sw, "Reporting physisorption data for gas/solid systems with special reference to the determination of surface area and porosity (Recommendations 1984)," *Pure and Applied Chemistry*, vol. 57, 1985.

[27] M. Betancur, J. D. Martínez, and R. Murillo, "Production of activated carbon by waste tire thermochemical degradation with CO2," *Journal of Hazardous Materials*, vol. 168, no. 2-3, pp. 882–887, 2009.

[28] B. Prakashkumar, K. Shivakamy, L. Miranda, and M. Velan, "Preparation of steam activated carbon from rubberwood sawdust (Hevea brasiliensis) and its adsorption kinetics," *Journal of Hazardous Materials*, vol. 136, no. 3, pp. 922–929, 2006.

[29] M. Keiluweit, P. S. Nico, M. G. Johnson, and M. Kleber, "Dynamic molecular structure of plant biomass-derived black

carbon (biochar)," *Environmental Science and Technology*, vol. 44, no. 4, pp. 1247–1253, 2010.

[30] X. Wang, C. Chen, W. Hu, A. Ding, D. Xu, and X. Zhou, "Sorption of 243Am(III) to multiwall carbon nanotubes," *Environmental Science and Technology*, vol. 39, no. 8, pp. 2856–2860, 2005.

[31] M. Ahmad, S. S. Lee, X. Dou et al., "Effects of pyrolysis temperature on soybean stover- and peanut shell-derived biochar properties and TCE adsorption in water," *Bioresource Technology*, vol. 118, pp. 536–544, 2012.

[32] T. Chen, C. Deng, and R. Liu, "Effect of selective condensation on the characterization of bio-oil from pine sawdust fast pyrolysis using a fluidized-bed reactor," *Energy and Fuels*, vol. 24, no. 12, pp. 6616–6623, 2010.

[33] J.-H. Zhou, Z.-J. Sui, J. Zhu et al., "Characterization of surface oxygen complexes on carbon nanofibers by TPD, XPS and FT-IR," *Carbon*, vol. 45, no. 4, pp. 785–796, 2007.

[34] J. L. Hueso, J. P. Espinós, A. Caballero, J. Cotrino, and A. R. González-Elipe, "XPS investigation of the reaction of carbon with NO, O2, N2 and H2O plasmas," *Carbon*, vol. 45, no. 1, pp. 89–96, 2007.

[35] N. Graf, E. Yegen, T. Gross et al., "XPS and NEXAFS studies of aliphatic and aromatic amine species on functionalized surfaces," *Surface Science*, vol. 603, no. 18, pp. 2849–2860, 2009.

[36] Z. Zhan, J. Dai, X. Wu, W. Zhang, K. Wang, and S. Yuan, "Adsorption of tetracycline and chloramphenicol in aqueous solutions by bamboo charcoal: a batch and fixed-bed column study," *Chemical Engineering Journal*, vol. 228, 2013.

[37] T. R. Bastami and M. H. Entezari, "Activated carbon from carrot dross combined with magnetite nanoparticles for the efficient removal of p-nitrophenol from aqueous solution," *Chemical Engineering Journal*, vol. 210, pp. 510–519, 2012.

[38] D. Robati, M. Rajabi, O. Moradi et al., "Kinetics and thermodynamics of malachite green dye adsorption from aqueous solutions on graphene oxide and reduced graphene oxide," *Journal of Molecular Liquids*, vol. 214, pp. 259–263, 2016.

[39] L. Hong, "Preparation of pickling-reheating activated alfalfa biochar with high adsorption efficiency for p-nitrophenol: characterization, adsorption behavior, and mechanism," *Environmental Science & Pollution Research International*, vol. 26, 2019.

[40] A. E. Ofomaja, "Kinetics and pseudo-isotherm studies of 4-nitrophenol adsorption onto mansonia wood sawdust," *Industrial Crops and Products*, vol. 33, no. 2, pp. 418–428, 2011.

[41] L. J. E. Science and P. R. International, "Preparation of pickling-reheating activated alfalfa biochar with high adsorption efficiency for p-nitrophenol: characterization, adsorption behavior, and mechanism," *Environmental Science & Pollution Research International*, vol. 26, 2019.

[42] N. Modirshahla, "Investigation of the efficiency of ZnO photocatalyst in the removal of p-nitrophenol from contaminated water," *Iranian Journal of Chemistry and Chemical Engineering (International English Edition)*, vol. 18, 2009.

[43] N. Zandi-Atashbar, A. A. Ensafi, and A. H. Ahoor, "Magnetic Fe2CuO4/rGO nanocomposite as an efficient recyclable catalyst to convert discard tire into diesel fuel and as an effective mercury adsorbent from wastewater," *Journal of Cleaner Production*, vol. 172, pp. 68–80, 2018.

[44] B. Jović, B. Kordić, V. Miškov, J. Tričković, M. Kovačević, and S. Petrović, "Amides as a model system of low molar mass algal organic matter. Influence on the adsorption of p-nitrophenol on activated carbon," *Arabian Journal of Chemistry*, vol. 13, no. 1, pp. 59–66, 2020.

[45] Y. Yue, Y. Wang, C. Qu, and X. Xu, "Modification of polyacrylonitrile-based activated carbon fibers and their p-nitrophenol adsorption and degradation properties," *Journal of Environmental Chemical Engineering*, vol. 9, no. 4, Article ID 105390, 2021.